



A Heat Shock Protein 48 (HSP48) Biomolecular Condensate Is Induced during *Dictyostelium discoideum* Development

Stephanie Santarriaga,^a Alicia Fikejs,^a Jamie Scaglione,^b  K. Matthew Scaglione^{a*}

^aDepartment of Biochemistry, Medical College of Wisconsin, Milwaukee, Wisconsin, USA

^bDepartment of Computational and Physical Sciences, Carroll University, Waukesha, Wisconsin, USA

ABSTRACT The social amoeba *Dictyostelium discoideum*'s proteome contains a vast array of simple sequence repeats, providing a unique model to investigate proteostasis. Upon conditions of cellular stress, *D. discoideum* undergoes a developmental process, transitioning from a unicellular amoeba to a multicellular fruiting body. Little is known about how proteostasis is maintained during *D. discoideum*'s developmental process. Here, we have identified a novel α -crystallin domain-containing protein, heat shock protein 48 (HSP48), that is upregulated during *D. discoideum* development. HSP48 functions in part by forming a biomolecular condensate via its highly positively charged intrinsically disordered carboxy terminus. In addition to HSP48, the highly negatively charged primordial chaperone polyphosphate is also upregulated during *D. discoideum* development, and polyphosphate functions to stabilize HSP48. Upon germination, levels of both HSP48 and polyphosphate dramatically decrease, consistent with a role for HSP48 and polyphosphate during development. Together, our data demonstrate that HSP48 is strongly induced during *Dictyostelium discoideum* development. We also demonstrate that HSP48 forms a biomolecular condensate and that polyphosphate is necessary to stabilize the HSP48 biomolecular condensate.

IMPORTANCE During cellular stress, many microbes undergo a transition to a dormant state. This includes the social amoeba *Dictyostelium discoideum* that transitions from a unicellular amoeba to a multicellular fruiting body upon starvation. In this work, we identify heat shock protein 48 (HSP48) as a chaperone that is induced during development. We also show that HSP48 forms a biomolecular condensate and is stabilized by polyphosphate. The findings here identify *Dictyostelium discoideum* as a novel microbe to investigate protein quality control pathways during the transition to dormancy.

KEYWORDS *Dictyostelium discoideum*, chaperone, phase separation, small heat shock protein

Upon cellular stress, cells elicit a number of responses, such as the induction of stress responsive genes, reduced translation, formation of phase-separated compartments, including stress granules, and the production of the chemical chaperone polyphosphate (1–10). Activation of these pathways provides defense mechanisms for cells to combat protein aggregation and promote cell survival. In addition to activating stress pathways upon experiencing cellular stress, some organisms enter dormancy, allowing them to survive adverse conditions, including extreme temperatures, desiccation, and starvation (11, 12).

One organism that enters a dormant state is the social amoeba *Dictyostelium discoideum*. Under conditions of cellular stress, *D. discoideum* undergoes a developmental process transitioning from a single cellular amoeba to a multicellular fruiting body containing dormant spores (13, 14). *D. discoideum* spores, which consist of a thick


Citation Santarriaga S, Fikejs A, Scaglione J, Scaglione KM. 2019. A heat shock protein 48 (HSP48) biomolecular condensate is induced during *Dictyostelium discoideum* development. *mSphere* 4:e00314-19. <https://doi.org/10.1128/mSphere.00314-19>.

Editor Aaron P. Mitchell, Carnegie Mellon University

Copyright © 2019 Santarriaga et al. This is an open-access article distributed under the terms of the [Creative Commons Attribution 4.0 International license](https://creativecommons.org/licenses/by/4.0/).

Address correspondence to K. Matthew Scaglione, matt.scaglione@duke.edu.

* Present address: K. Matthew Scaglione, Department of Molecular Genetics and Microbiology, Department of Neurology, and Duke Center for Neurodegeneration and Neurotherapeutics, Duke University School of Medicine, Durham, North Carolina, USA.

 HSP48 is induced during *Dictyostelium discoideum* development and forms a biomolecular condensate. @scaglione1ab

Received 30 April 2019

Accepted 4 June 2019

Published 19 June 2019

cellulose-rich spore encapsulating a dehydrated amoeba, can withstand unfavorable conditions such as extreme temperatures and desiccation (11). This developmental process allows *D. discoideum* to survive until environmental conditions have improved and the spores can germinate into amoeba (15).

One largely unexplored question is how proteostasis is maintained upon entry into dormancy. This is particularly interesting in the case of *D. discoideum*, as it encodes a proteome that contains a large number of repetitive amino acid tracts that are known to aggregate in other model organisms (16–18). Molecular chaperones, including the ATP-dependent foldases and the α -crystallin domain-containing holdases, are often upregulated upon cellular stress and play a protective role in maintaining proteostasis (19–21). Though it is known that *D. discoideum* harbors a large number of α -crystallin domain-containing proteins, their function in *D. discoideum* remains largely unexplored (16).

In addition to protein quality control pathways, the formation of stress-triggered biomolecular condensates also plays a protective role during cellular stress (2, 22–25). Biomolecular condensates are highly spherical membraneless compartments that comprise a variety of biological processes ranging from nucleolus formation to cellular signaling (26–32). Proteins that phase separate to form biomolecular condensates often contain intrinsically disordered domains that can enable liquid-liquid phase separation (5, 6, 27, 29, 33–36). In addition to intrinsically disordered domains, highly charged regions of proteins also drive phase separation via complementary electrostatic interactions (5, 37–41).

While little is known about stress responses during *D. discoideum* development, one potential chaperone that is increased during development is the chemical chaperone polyphosphate (10, 42). Polyphosphate plays a number of important roles in *D. discoideum* development, including regulating metabolism, spore germination, and fitness (10). In addition to its intracellular effects on *D. discoideum* development, excreted polyphosphate also promotes development by inhibiting proliferation and signaling through Ras and Akt (8, 9). In other model organisms, polyphosphate functions as a chaperone promoting the productive refolding of misfolded proteins and stabilizing amyloid fibers (43, 44).

How *D. discoideum*'s proteostatic network maintains proteostasis during its developmental cycle is largely unexplored. Here, we identify an uncharacterized α -crystallin domain-containing protein we named heat shock protein 48 (HSP48) whose transcript level is greatly induced during *D. discoideum* development. In cells, HSP48 undergoes liquid-liquid phase separation to form a biomolecular condensate in cells. In addition to HSP48's N-terminal α -crystallin domain, HSP48 also contains a highly positively charged C terminus that is required for phase separation. In addition to HSP48 transcript, levels of the highly negatively charged primordial chaperone polyphosphate are also sharply increased during *D. discoideum* development, and polyphosphate is necessary to stabilize HSP48 protein levels. Upon germination, both HSP48 transcript and polyphosphate levels are rapidly diminished. Together, our data are consistent with a coordinated role for the molecular chaperone HSP48 and the chemical chaperone polyphosphate during *D. discoideum* development.

RESULTS

HSP48 is highly expressed during *D. discoideum* development. We previously discovered that *D. discoideum* contains a large number of α -crystallin domain-containing proteins, including four previously unidentified α -crystallin domain-containing proteins (Table 1) (16). α -Crystallin domain-containing proteins have been implicated in the developmental process of some bacteria, leading us to hypothesize that they may also participate in *D. discoideum* development (45, 46). To begin assessing protein quality control pathways in *D. discoideum* development, we measured the expression levels of α -crystallin domain-containing proteins in the amoeba and upon completion of development. We identified one uncharacterized α -crystallin domain-containing protein, HSP48, whose transcript levels were induced greater than 1,000-fold in fruiting bodies

TABLE 1 Newly identified α -crystallin-domain containing proteins

Gene name	Gene ID ^a
<i>hsp19</i>	DDB_G0295803
<i>hsp48</i>	DDB_G0280215
<i>hsp69</i>	DDB_G0283911
<i>hsp83</i>	DDB_G0288861

^aID, identifier.

compared to that in the amoeba (Fig. 1A). Unlike most other α -crystallin domain-containing proteins, such as HSPG1 and HSPG2, HSP48 expression did not increase upon heat stress, suggesting a more selective role in development (Fig. 1B). This suggests that HSP48 may play an important role in *D. discoideum* development.

HSP48 forms a biomolecular condensate *in vivo*. Molecular chaperones can exist in various cellular compartments, including the endoplasmic reticulum, the nucleus, the cytoplasm, and the spore coat of developing bacteria (45–47). To determine HSP48's cellular localization, we generated a green fluorescent protein (GFP)-tagged HSP48 construct (GFP-HSP48) and expressed it in *D. discoideum* cells. GFP-HSP48 was present in the cytosol; however, rather than being diffuse, it formed puncta in cells (Fig. 2A). To assess the sphericity of GFP-HSP48 puncta, we obtained z-stacks of GFP-HSP48 puncta and analyzed three-dimensional (3D) reconstituted images using Imaris software (Fig. 2A). Consistent with HSP48 forming nearly perfect spheres, the mean average sphericity of GFP-HSP48 was calculated to be >0.95 (Fig. 2B). The GFP-HSP48 puncta did not appear to colocalize with the nucleus, lysosome, or *trans*-Golgi (Fig. 2C to E), suggesting that HSP48 may undergo liquid-liquid phase separation. Because protein aggregates may also form spherical structures, we next wanted to measure the dynamics of HSP48 spheres. Unlike protein aggregates where proteins are highly immobile in a solid-like

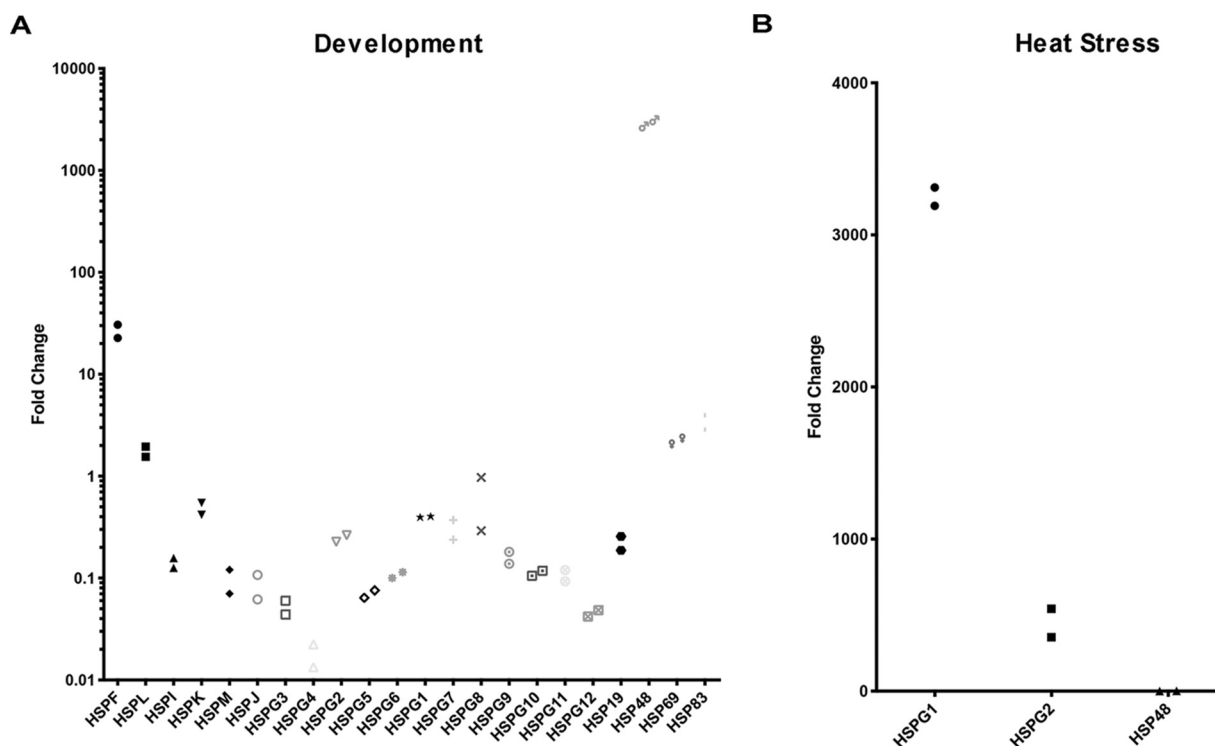


FIG 1 HSP48 is upregulated during *Dictyostelium discoideum* development. (A) HSP48 expression is upregulated during *Dictyostelium* development. Wild-type *Dictyostelium* cells were starved to induce development. Cells were harvested at 0 and 24 h for RNA extraction, and RT-PCR was performed to assess expression levels of α -crystallin domain-containing proteins ($n = 2$). (B) HSP48 is not induced upon heat stress. Wild-type *Dictyostelium* cells were grown at either 22°C or 30°C for 1 h and then harvested for RNA extraction. RT-PCR was performed to assess expression levels of the α -crystallin domain-containing proteins HSPG1, HSPG2, and HSP48 ($n = 2$).

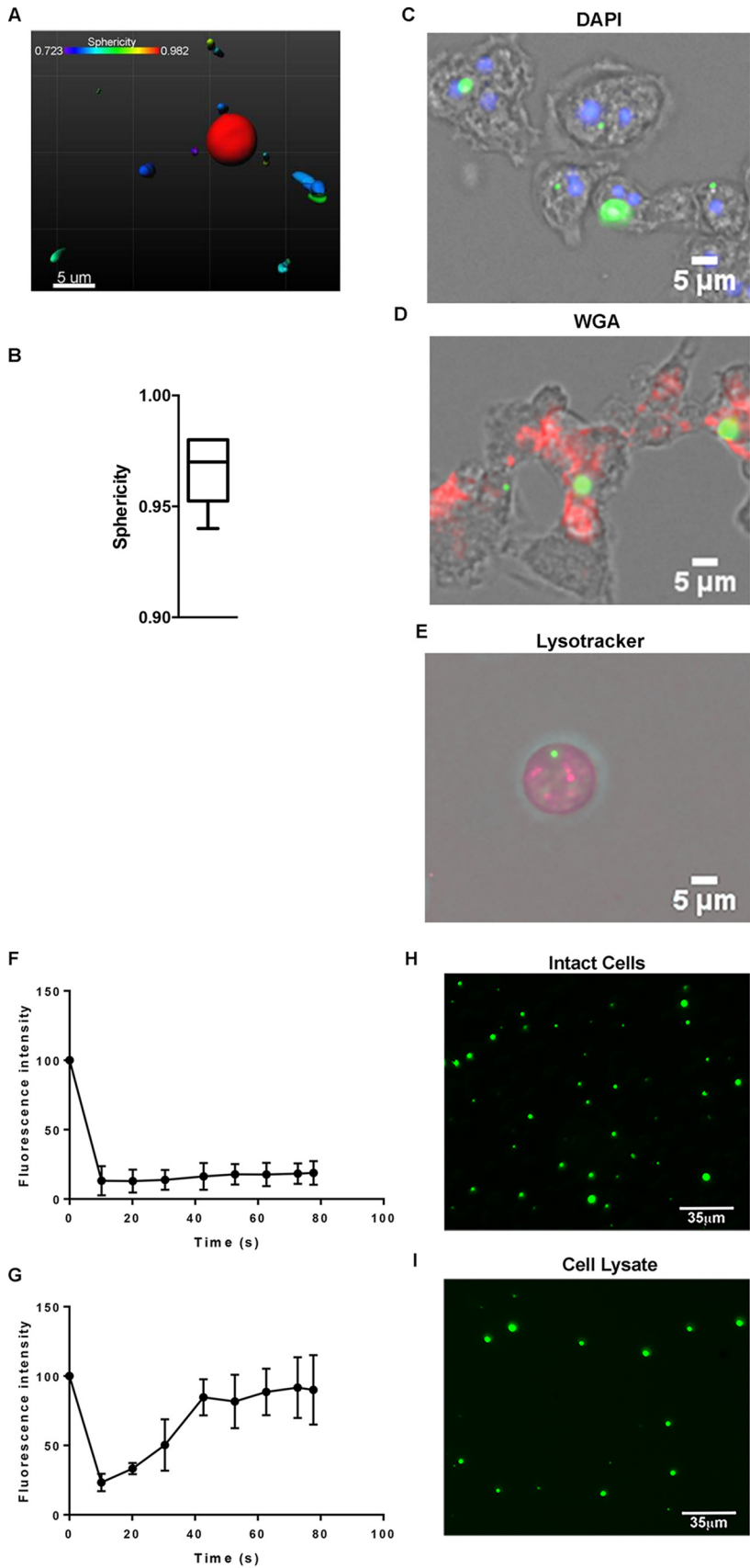


FIG 2 HSP48 phase separates to form a biomolecular condensate. (A) 3D volume-rendered HSP48. *Dictyostelium* cells expressing ^{GFP}HSP48 were imaged using a confocal microscope. 3D volumes were (Continued on next page)

state, biomolecular condensates are present in both highly dynamic liquid-like states and more glass-like solid states (26). To determine if HSP48 was in either a liquid or solid state, we next performed fluorescence recovery after photobleaching (FRAP) analysis on ^{GFP}HSP48 puncta. In our FRAP analysis, half of a ^{GFP}HSP48 biomolecular condensate was bleached, and recovery of fluorescence in the bleached area was then measured over time. Similarly to other biomolecular condensates, we observed multiple states for ^{GFP}HSP48 with one population (~72%) behaving more solid like (less mobility within the condensate) (Fig. 2F) and a second population (~28%) behaving more liquid like (more mobility within the condensate) (Fig. 2G) (48, 49). Additionally, unlike membrane-bound organelles and vesicles, biomolecular condensates form compartments that do not require a lipid bilayer (4, 29, 50). To determine if HSP48 puncta formation required a lipid bilayer, we disrupted lipid bilayers with detergent and looked to see if ^{GFP}HSP48 remained as puncta in the cell lysates. Consistent with HSP48 puncta being a membraneless structure, ^{GFP}HSP48 puncta remained after cell lysis with detergent (Fig. 2H and I). Together, these data suggest that HSP48 forms a biomolecular condensate in the cytoplasm of *D. discoideum*.

HSP48's intrinsically disordered C-terminal region is necessary for biomolecular condensate formation. One common characteristic of proteins that form biomolecular condensates is the presence of an intrinsically disordered domain (5, 6, 27–29, 31, 37, 38, 51–54). To determine if HSP48 has an intrinsically disordered domain, we performed *in silico* analysis of HSP48's sequence using multiple algorithms, including RONN, PONDR, FoldIndex, and IUPred. With each algorithm, a region next to the C terminus of HSP48 was predicted to be intrinsically disordered (Fig. 3A to D). We next wanted to determine if HSP48's intrinsically disordered domain is responsible for driving its phase separation. To accomplish this, we made HSP48 constructs with deletions of either the C-terminal intrinsically disordered domain (^{GFP}HSP48^{ΔC-term}) or HSP48's N-terminal α -crystallin domain (^{GFP}HSP48^{ΔN-term}) and tested their ability to form biomolecular condensates in cells (Fig. 3E). Consistent with a region next to HSP48's C terminus driving phase separation, ^{GFP}HSP48^{ΔC-term} did not form a biomolecular condensate but instead was diffuse, while both wild-type ^{GFP}HSP48 and the ^{GFP}HSP48^{ΔN-term} retained their ability to form puncta in cells (Fig. 3F). Consistent with our *in vivo* data, ^{GFP}HSP48 and ^{GFP}HSP48^{ΔN-term} puncta remained after cell lysis, while ^{GFP}HSP48^{ΔC-term} was diffuse (Fig. 3G). Together, these data demonstrate that the formation of an HSP48 biomolecular condensate is driven by the region next to its C terminus.

Polyphosphate regulates HSP48 phase separation and stability. We next wanted to understand how this region next to HSP48's C terminus drives biomolecular condensate formation. Previous work demonstrated that complementary electrostatic interactions drive the formation of many biomolecular condensates (5, 37–41), and so we analyzed the region next to HSP48's C terminus to identify charged regions. Using

FIG 2 Legend (Continued)

then produced using Imaris software. (B) HSP48 puncta are highly spherical. 3D volume images of HSP48 were used to obtain sphericity values using Imaris software. Values equal to 1 indicate sphericity ($n = 20$). (C) HSP48 colocalizes to defined puncta. *Dictyostelium* cells were electroporated with a plasmid that expresses ^{GFP}HSP48 and selected for a minimum of 2 weeks. Cells were fixed with methanol, stained with DAPI, and imaged with a fluorescence microscope ($n = 3$). (D) HSP48 colocalizes to defined puncta. *Dictyostelium* cells were electroporated with a plasmid that expresses ^{GFP}HSP48 and selected for a minimum of 2 weeks. Cells were fixed with methanol, stained with wheat germ agglutinin (WGA), and imaged with a fluorescence microscope ($n = 3$). (E) HSP48 colocalizes to defined puncta. *Dictyostelium* cells were electroporated with a plasmid that expresses ^{GFP}HSP48 and selected for a minimum of 2 weeks. Cells were stained with LysoTracker and imaged live with a fluorescence microscope ($n = 3$). (F and G) HSP48 FRAP analysis reveals two populations with different inherent mobilities. *Dictyostelium* cells were electroporated with a plasmid that expresses ^{GFP}HSP48, selected for a minimum of 2 weeks, and used for FRAP. For FRAP, half of each individual droplet was bleached and then imaged for the indicated time points. ImageJ was then used for analysis to obtain fluorescence intensity values ($n = 18$). HSP48 puncta do not require a lipid bilayer. *Dictyostelium* cells were electroporated with a plasmid that expresses ^{GFP}HSP48 and selected for a minimum of 2 weeks. Cells were either imaged as intact cells (H) or lysed (I) and imaged by fluorescence microscopy ($n = 5$).

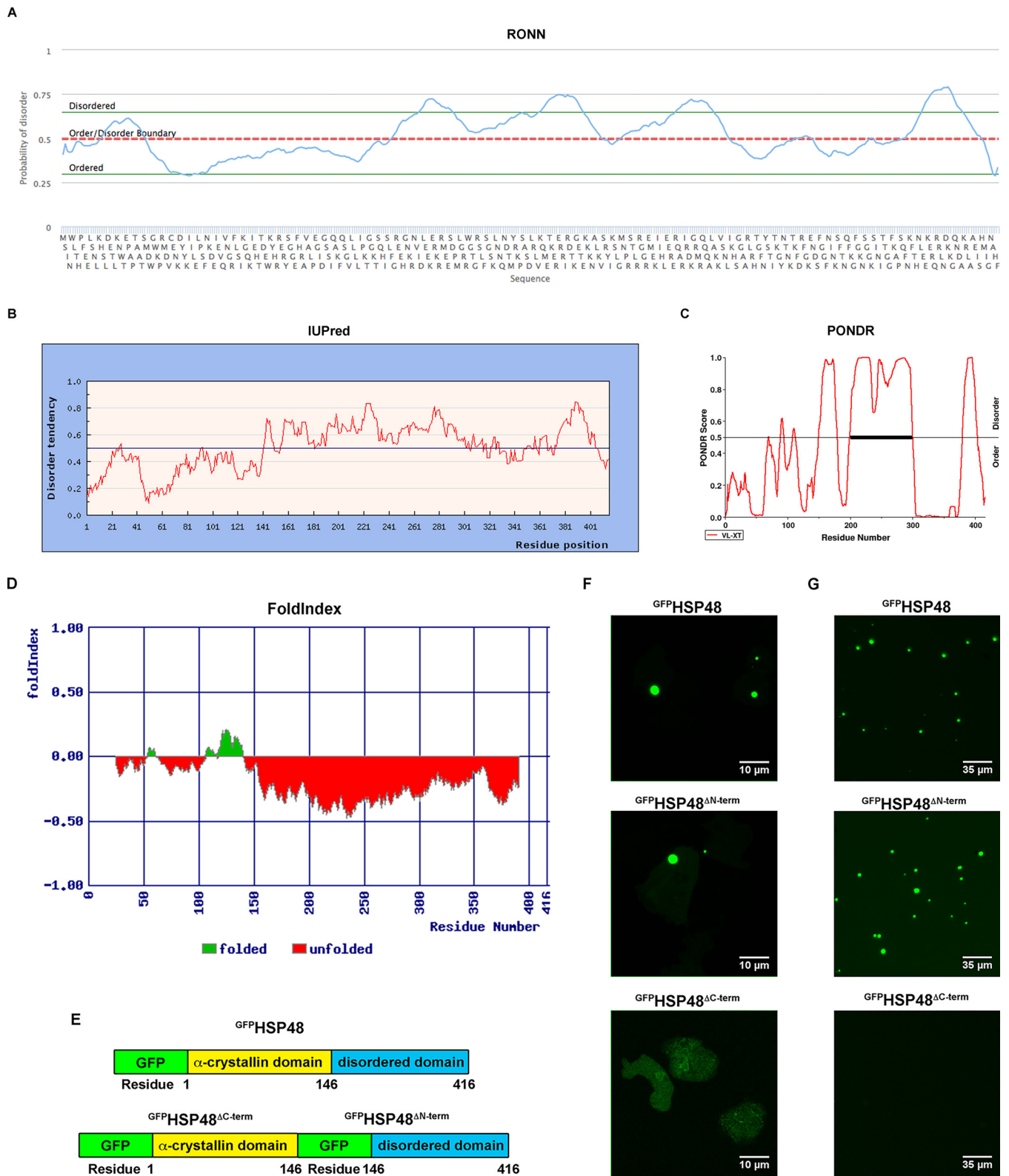


FIG 3 A region next to HSP48's C terminus drives phase separation. A region next to HSP48's C terminus is intrinsically disordered. HSP48's amino acid sequence was analyzed for its probability of disorder using RONN (A), IUPred (B), PONDR (C), and FoldIndex (D). (E and F) HSP48's intrinsically disordered region is necessary for liquid droplet formation. *Dictyostelium* cells were electroporated with plasmids that express either GFPHSP48, GFPHSP48 Δ N-term, or GFPHSP48 Δ C-term and selected for a minimum of 2 weeks. Cells were then imaged using confocal microscopy ($n = 3$). (G) HSP48 puncta do not require a lipid bilayer. *Dictyostelium* cells were electroporated with plasmids that express either GFPHSP48, GFPHSP48 Δ N-term, or GFPHSP48 Δ C-term and selected for a minimum of 2 weeks. Cells were then lysed and imaged using a fluorescence microscope ($n = 5$).

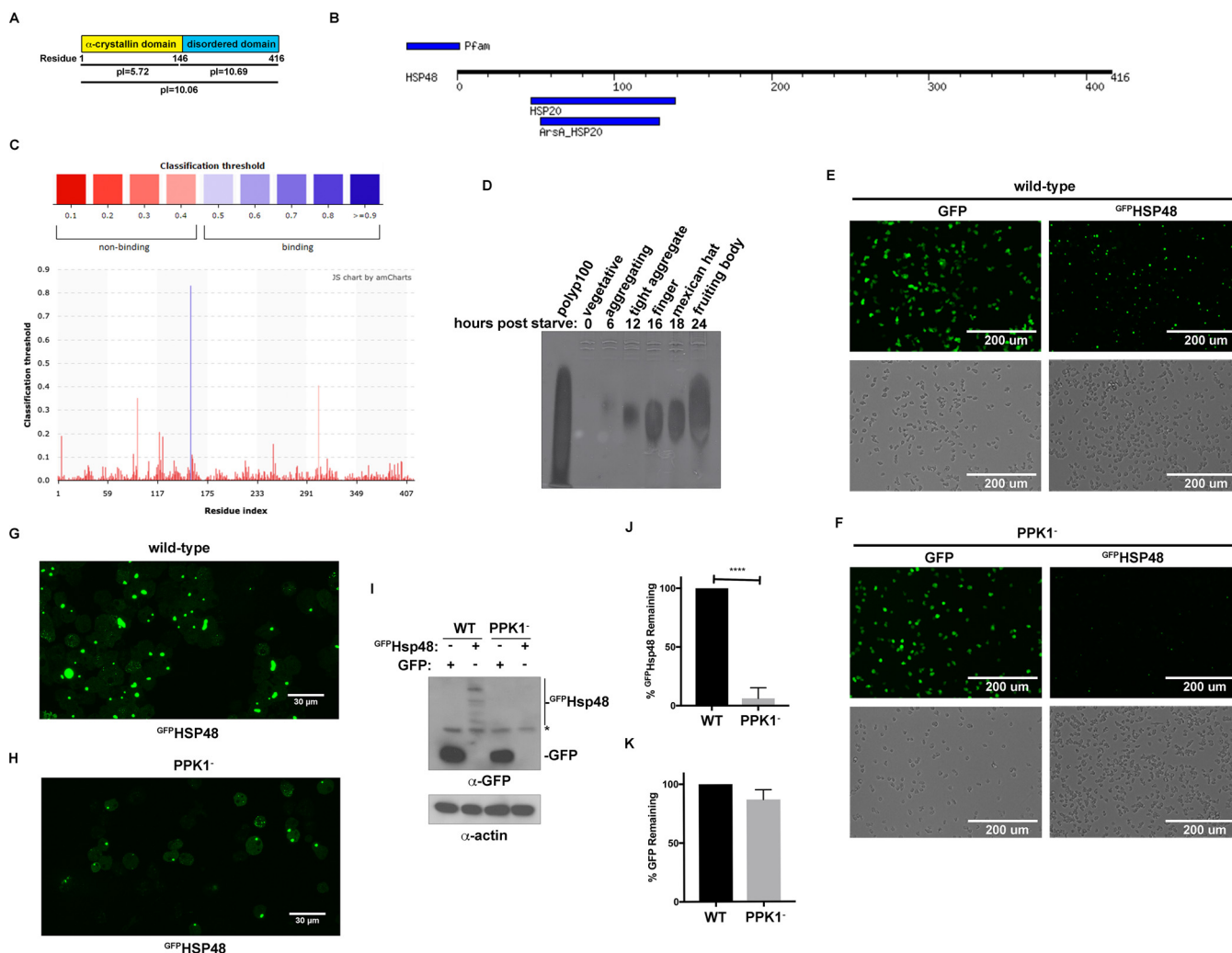


FIG 4 Polyphosphate drives HSP48 phase separation and stabilization. (A) HSP48 has a highly basic C terminus. *In silico* analysis of HSP48 was performed to determine the isoelectric point. (B) HSP48 is not predicted to have a DNA or RNA binding motif. HSP48's amino acid sequence was analyzed by MOTIF search against the Pfam database. (C) HSP48 is not predicted to bind RNA. HSP48's amino acid sequence was analyzed by PRIdictor. (D) Polyphosphate levels increase during *Dictyostelium* development. Wild-type AX4 cells were developed and harvested at the indicated time points. To image polyphosphate, RNA was isolated, run on an acrylamide gel, and stained with DAPI ($n = 3$). (E, F) Polyphosphate promotes HSP48 phase separation *in vivo*. ^{GFP}HSP48 constructs were transformed into wild-type (C) and Δ PPK1 (PPK1⁻) (D) cells. Cells were selected and then imaged using a fluorescence microscope ($n = 4$). (G) Confocal image of ^{GFP}HSP48 puncta in wild-type cells. Wild-type cells electroporated with a plasmid that expresses ^{GFP}HSP48 and were imaged by confocal microscopy ($n = 4$). (H) Confocal image of ^{GFP}HSP48 puncta in Δ PPK1 cells. Δ PPK1 cells were electroporated with a plasmid that expresses ^{GFP}HSP48 and were imaged by confocal microscopy ($n = 4$). (I) ^{GFP}HSP48 protein levels are decreased in Δ PPK1 cells. Wild-type and Δ PPK1 cells expressing either ^{GFP}HSP48 or GFP were analyzed by Western blotting ($n = 3$). *, nonspecific band. (J) ^{GFP}HSP48 protein levels are decreased in Δ PPK1 cells. Quantification of HSP48 in wild-type and Δ PPK1 cells ($n = 3$). ****, $P < 0.0001$. (K) GFP protein levels are unchanged in Δ PPK1 cells. Quantification of GFP in wild-type and Δ PPK1 cells ($n = 3$).

in silico analysis, we found that the intrinsically disordered region next to HSP48's C terminus is highly basic with an isoelectric point of 10.69, while HSP48's N-terminal α -crystallin domain has an isoelectric point of 5.72 (Fig. 4A). One common negatively charged molecule that drives the formation of biomolecular condensates is RNA (5, 6, 28, 29, 36, 37, 52, 55). To determine if HSP48 contained any predicted RNA-binding motifs, we next performed an *in silico* analysis using MOTIF and PRIdictor (56, 57); however, neither program identified an RNA-binding domain within HSP48 (Fig. 4B and C).

Because HSP48 lacked a predicted RNA-binding motif, we hypothesized another highly acidic molecule may be driving HSP48 phase separation. Because HSP48 accumulates during development, we turned our attention to polyphosphate, a highly negatively charged molecule whose levels dramatically increase during *D. discoideum* development (10). To confirm that polyphosphate levels increase during *D. discoideum*

development, we induced *D. discoideum* development by starvation and analyzed polyphosphate accumulation at 0, 6, 12, 16, 18, and 24 h by using an established technique (10). Consistent with previous studies, we found that polyphosphate levels increased during *D. discoideum* development similarly to HSP48 (10) (Fig. 4D). To determine if polyphosphate was necessary for HSP48 phase separation, we expressed ^{GFP}HSP48 in *D. discoideum* cells lacking polyphosphate kinase 1 (PPK1), the major enzyme responsible for polyphosphate production in *D. discoideum* (10). In Δ PPK1 cells, the size and number of the ^{GFP}HSP48 biomolecular condensates formed were dramatically decreased (Fig. 4E to H). In addition to decreasing ^{GFP}HSP48 puncta, we also observed a decrease in diffuse ^{GFP}HSP48, suggesting that ^{GFP}HSP48 is destabilized in the absence of polyphosphate (Fig. 4E to H). Western blot analysis of wild-type and Δ PPK1 cells expressing ^{GFP}HSP48 verified that while the GFP control remained unchanged, ^{GFP}HSP48 levels were decreased in Δ PPK1 cells, suggesting a potential role for polyphosphate in regulating HSP48 protein levels (Fig. 4I). Because polyphosphate plays a role in regulating transcription and translation (58–60), we wanted to confirm that ^{GFP}HSP48 destabilization was not due to differences in transcription and translation. Consistent with no change in HSP48 transcription or translation, fluorescence levels were similar in wild-type and Δ PPK1 cells expressing GFP alone, indicating that global transcription and translation were not altered (Fig. 4E to K). Because transcription and translation were unaffected, this suggested that polyphosphate may be functioning to stabilize HSP48 by preventing its degradation. Together, these data are consistent with a role for polyphosphate in stabilizing ^{GFP}HSP48 by preventing its clearance.

We observed that transcript levels for HSP48 were dramatically increased upon *D. discoideum* development (Fig. 1A), and we and others have observed that polyphosphate levels are robustly upregulated during *D. discoideum* development (Fig. 4D) (10). We next wanted to determine if polyphosphate and HSP48 transcript levels are downregulated upon germination of *D. discoideum* spores. To accomplish this, we analyzed *D. discoideum* spores and amoeba that had been allowed to germinate for 5 h, a time point where greater than 95% of spores had germinated (Fig. 5A and B). Consistent with polyphosphate levels dramatically decreasing upon germination, polyphosphate was undetectable 5 h after the addition of nutrients (Fig. 5C). We next wanted to determine if HSP48 transcript levels also decreased upon germination. To determine this, we assessed HSP48 transcript levels in spores and amoeba 5 h after induction of germination. Consistent with HSP48 transcript levels being downregulated upon germination, we detected nearly no HSP48 transcript in germinated cells (Fig. 5D). Together, these data are consistent with a rapid downregulation of both HSP48 and polyphosphate upon germination of *D. discoideum* spores.

DISCUSSION

Here, we identify HSP48 as a novel α -crystallin domain-containing protein that is vastly upregulated during *D. discoideum* development (Fig. 1). HSP48 forms a biomolecular condensate, a process dependent on its highly basic intrinsically disordered region next to the C terminus (Fig. 2 and 3). The highly acid chemical chaperone, polyphosphate, is necessary to stabilize HSP48, and deletion of PPK1, the major enzyme responsible for polyphosphate production in *D. discoideum*, results in a destabilization of HSP48 levels (Fig. 4). Finally, upon germination, levels of both HSP48 transcript and polyphosphate are dramatically decreased, consistent with their role in development (Fig. 5). Moving forward, it will be important to determine if HSP48 is essential for *D. discoideum* development and, if so, what role it plays.

How *D. discoideum* maintain proteostasis during their developmental process is largely unknown. However, it is known that protein degradation pathways are essential for *D. discoideum* development. Deletion of autophagy genes, including *atg1*, *atg5*, *atg6*, *atg7*, and *atg8*, or of the deubiquitinating enzyme UbpA results in abnormal development (61–63). Similarly, the molecular chaperone Hsp90 is also necessary for *D. discoideum* development, as Hsp90 inhibition with geldanamycin arrests *D. discoideum*

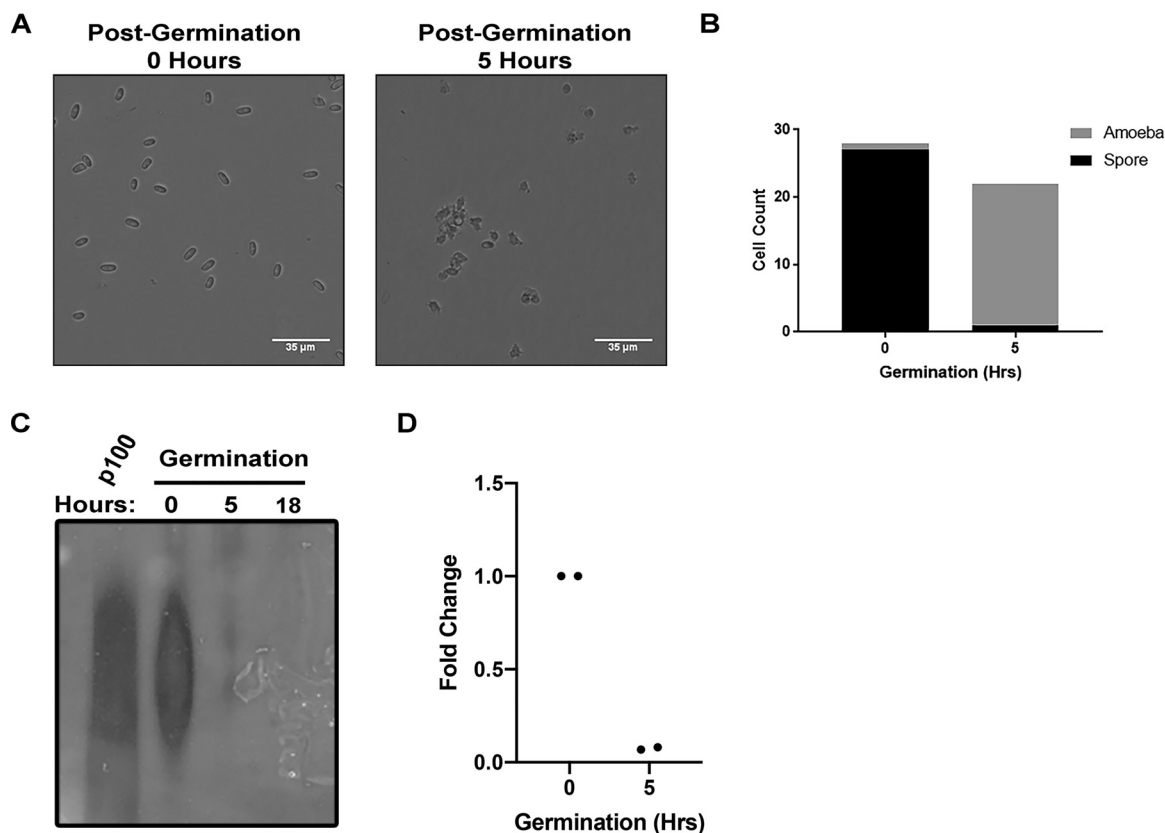


FIG 5 Polyphosphate and HSP48 levels dramatically decrease upon germination. (A) Wild-type AX4 cells were developed for 24 h, after which, spores were isolated and cultured in medium for the indicated time points. Cells were then imaged using bright-field microscopy. (B) Quantification of the numbers of amoeba and spores at 0 h (number of cells counted = 28) and 5 h postgermination (number of cells counted = 22). (C) Polyphosphate decreases rapidly after germination. Wild-type AX4 cells were developed for 24 h, after which, spores were isolated and cultured in medium for the indicated time points. RNA was extracted to obtain polyphosphate, run on an acrylamide gel, and stained with DAPI ($n = 3$). (D) HSP48 transcript levels decrease rapidly after germination. Wild-type AX4 cells were developed for 24 h, after which, spores were isolated and cultured in medium for the indicated time points. RNA was extracted, and RT-PCR was performed to assess expression levels of HSP48 ($n = 3$).

development at the mound stage (64). However, it is unclear if the defects in development result from a broad disruption in proteostasis or from a disruption of select pathways. While we observed a large induction of HSP48 during *D. discoideum* development (Fig. 1), levels of another α -crystallin domain-containing protein, HSP32, decreased, suggesting that components of the proteostatic network may be tightly regulated during *D. discoideum* development (65). Because HSP48 is an α -crystallin domain-containing protein, it will be important to identify its role in maintaining proteostasis during *D. discoideum* development. Moving forward, it will be interesting to identify other protein quality control components that help maintain proteostasis during development. This will be particularly interesting in *D. discoideum* spores, as their highly compact desiccated environment presents unique challenges in maintaining proteostasis.

Though *D. discoideum* development provides a unique model for interrogating protein quality control pathways, HSP48 also provides a potential model for studying phase separation. In recent years, phase separation has been identified as a mechanism to regulate transcription and protein aggregation under various conditions (25, 66–68). Stress granules, which have become the primary system for studying membraneless organelles and phase separation, have been greatly associated with neurodegenerative diseases, as an increasing number of disease-associated proteins have been shown to phase separate (6, 7, 26, 28, 36, 41, 69–72). For instance, the identification of a liquid-to-solid-phase transition with disease-associated FUS mutations led to the rec-

ognition of aberrant phase separation as a major contributing factor in amyotrophic lateral sclerosis (ALS) (28, 36, 41). Additionally, the phase separation of individual proteins has now been tied back to other major diseases, such as the polyglutamine diseases and Alzheimer's disease (39, 40, 52, 69, 73, 74). Interestingly, the resulting solid states of phase-separated proteins greatly resemble protein fibrils seen in disease. However, it is unclear whether phase separation functions as a mechanism for amyloid fibril formation or whether it functions as an independent pathway. A greater understanding of this process is necessary for the development of therapeutics for neurodegenerative diseases associated with aberrant phase separation.

While aberrant phase separation is observed in many neurodegenerative diseases, it is also becoming clear that phase separation serves an important function during cellular stress (2, 23). For example, stress granules in response to various stressors often serve to increase cellular fitness, suggesting that phase separation may serve as a general stress response (22, 23). In a similar stress response, cells may enter a highly desiccated dormant state in which the cytosol phase transitions from a liquid to a glass-like state (12, 24, 75–77), slowing down dynamics within the cell. In this manner, phase separation may serve as a protective effect providing sufficient time for the sequestration and refolding of misfolded proteins (78). In line with this, the small heat shock protein Hsp42 utilizes a prion-like domain to sequester misfolded proteins and utilizes a second intrinsically disordered domain to regulate this process. Interestingly, removal of the second intrinsically disordered domain improves the chaperone function of Hsp42; however, both domains are needed to promote cellular fitness, suggesting that regulating the sequestration of misfolded proteins is equally important (66). We speculate that HSP48 may similarly phase separate and bind misfolded proteins, allowing HSP48 to sequester proteins and maintain their solubility during *D. discoideum* development. This raises the possibility for phase separation to serve as a stress response that functions to sequester proteins and maintain proteostasis.

Previous work has shown that electrostatic interactions between RNA and protein can induce phase separation. For example, stress granules form in part via electrostatic interactions between negatively charged RNA and positively charged regions of RNA-binding proteins (6). Here, we show that polyphosphate, a highly negatively charged molecule whose levels vastly increase during *D. discoideum* development, promotes HSP48's phase separation (Fig. 4). The formation of a polyphosphate-HSP48 biomolecular condensate raises the possibility that HSP48 may act as a chaperone in multiple ways. On the one hand, polyphosphate is a chemical chaperone that binds unfolded proteins and supports productive refolding upon resolution of cellular stress (44). HSP48's α -crystallin domain coupled with polyphosphate's role as a chemical chaperone may act as a chaperoning complex that helps maintain proteostasis during development. Alternatively, polyphosphate promotes the conversion of misfolded proteins to form amyloid fibrils (43). In this regard, HSP48 may sequester polyphosphate in a biomolecular condensate, thus preventing it from promoting the formation of amyloid during *D. discoideum* development. In the future, *D. discoideum* development may serve as a useful model organism to determine whether polyphosphate is protective or detrimental in diseases of protein misfolding.

In addition to preventing polyphosphate-induced aggregation, the formation of an HSP48 biomolecular condensate may also serve as storage mechanism for polyphosphate during development. In other organisms, membrane-bound organelles known as acidocalcisomes have been observed to store calcium and polyphosphate (79). More recently, polyphosphate (polyP) storage granules lacking a membrane were identified in *Acetonea longum* during sporulation (80). In *D. discoideum*, as cells enter dormancy, an HSP48 biomolecular condensate may serve as a membraneless compartment for polyphosphate storage, providing a mechanism by which metabolism may be regulated. In this manner, polyphosphate would be sequestered in spores as a readily available energy source upon germination. In addition to *D. discoideum*, a number of microbes undergo a developmental process during cellular stress leading to the formation of dormant spores. As polyphosphate storage has been implicated for survival in response

to various stressors, it would be interesting to see if phase separation serves as the main mechanism for sequestering polyphosphate, providing an additional avenue for targeting drug-resistant microbes.

MATERIALS AND METHODS

Expression constructs and antibodies. HSP48 (DDB_G0280215; [XP_641311.1](#)) was PCR amplified from *D. discoideum* cDNA and cloned into Pet28 and pTxGFP (Dictybase) using BamHI and XhoI. Anti-ubiquitin antibody was from Invitrogen (14-6078-82) and anti-GFP was from Life Technologies (A11122). Peroxidase-conjugated secondary antibodies were from Jackson ImmunoResearch. IgG-fluorescein isothiocyanate (FITC) secondary was used for immunostaining (sc-2010; Santa Cruz). β -Actin (PA121167; Pierce) was used as a loading control.

***Dictyostelium discoideum* cell culture and transformations.** *Dictyostelium discoideum* AX4 cells were maintained in shaking cultures at 22°C in HL5 medium. Cells were subcultured to maintain a density no greater than 6×10^6 cells/ml.

Transformations were performed as previously described (81). Briefly, 5×10^6 cells were washed with H-50 buffer (20 mM HEPES, 50 mM KCl, 10 mM NaCl, 1 mM $MgSO_4$, 5 mM $NaHCO_3$, 1 mM NaH_2PO_4 ; pH adjusted to 7.0 with HCl/NaOH). Cells were electroporated in a 1-mm cuvette (0.85 kV/25 μ F, 0.6 ms, twice with 5 s in between). Cells were selected with 10- μ g/ml G-418 for 1 week (82).

Development. To induce development, 2×10^8 cells were washed and grown on filter paper soaked with filtered developmental buffer (5 mM Na_2HPO_4 , 5 mM KH_2PO_4 , 1 mM $CaCl_2$, 2 mM $MgCl_2$; pH adjusted to 6.5 with HCl/NaOH) at 22°C (14). Cells were harvested at various time points for RNA isolation.

For microscopy, 2×10^8 cells were washed with development buffer and grown on KK2 plates (14). Cells were developed for various time points and imaged using a Leica MZFL3 fluorescence stereomicroscope.

Heat stress. Briefly, 1×10^7 cells were incubated in HL5 medium at a density of 1×10^6 cells/ml at either 22°C or 30°C for 1 h. Cells were then harvested and used for RNA isolation.

RNA isolation and cDNA synthesis. For RNA isolation, Qiagen's RNeasy Mini kit was used according to the manufacturer's instructions. An optional DNase digestion step was performed, and the elution step was performed with RNase-free water. Invitrogen's SuperScript III First-Strand Synthesis System for real-time PCR (RT-PCR) was used for cDNA synthesis according to the manufacturer's instructions.

RT-PCR. Real-time PCR was performed using iQ SYBR green supermix (170-8880; Bio-Rad) in 96-well plates (Pryme PCR, AVRT1; MidSci) sealed with adhesive seals (MSB1001; Bio-Rad) in an Eppendorf RealPlex². Data were analyzed using the Livak method.

Immunocytochemistry. Cells were harvested at various time points and plated on 24-well plates at a density of 7.5×10^5 cells/ml. Cells were allowed to settle and then fixed with cold 100% methanol for 10 min at -20°C. Cells were briefly washed to remove remaining methanol and incubated in blocking buffer (2% bovine serum albumin [BSA], 1% Triton X-100 in 1 \times phosphate-buffered saline [PBS]) for 30 min at room temperature. Cells were then incubated in primary antibody (1:2,000 in blocking buffer) overnight at 4°C. Cells were washed three times with PBT (0.1% Triton X-100, 0.5% BSA in 1 \times PBS) and then incubated in secondary (1:500 in blocking buffer) for 2 h at room temperature in the dark. Cells were washed three times with PBT and imaged using an Evos FL Auto microscope (Life Technologies).

Confocal microscopy. Briefly, 3×10^6 cells were plated on coverslips, allowed to settle, and then fixed with cold 100% methanol for 10 min at -20°C. Cells were washed and stained with DAPI (4',6-diamidino-2-phenylindole; Life Technologies). Coverslips were mounted with ProLong Gold Antifade reagent (Life Technologies) and imaged with a Leica TCS Sp5 confocal scope. Z-stack images were captured at $\times 63$ magnification at 0.5- μ m intervals and 1,024 \times 1,024 pixel resolution and merged using Fiji.

For live cell imaging, *D. discoideum* cells were plated on 2% low-melt agarose pads in starvation buffer. Slides were prepared as previously described. Cells were imaged with a Nikon Eclipse 90i confocal microscope at $\times 100$ magnification. Z-stack images were obtained at 0.5- μ m intervals and 1,024 \times 1,024 pixel resolution and merged using Fiji.

Fluorescence microscopy. For live cell imaging, cells were washed with starvation buffer (0.1 M MES [morpholineethanesulfonic acid], 0.2 mM $CaCl_2$, 2 mM $MgSO_4$, pH adjusted to 6.8 with HCl/NaOH) and imaged at $\times 20$ magnification using an Evos FL Auto microscope (Life Technologies) (83). For lysate imaging, 1×10^7 cells were lysed with NETN (0.5% Nonidet P-40, 150 mM NaCl, 50 mM Tris, and protease inhibitors [Roche Applied Science]) and sonicated using an ultrasonic cell disruptor 2 times for 10 s on ice at 30% output. Lysis was then confirmed by bright-field imaging before imaging fluorescence at $\times 20$ magnification using an Evos FL Auto microscope (Life Technologies).

Spore germination. AX4 cells were developed for 2 to 3 days. For spore isolation, developed cells were harvested, resuspended in 1 ml of 10 mM MES (pH adjusted to 6.5 with HCl or NaOH), and vortexed for 1 min. An additional 4 ml of buffer was added to cells and they were vortexed again for 1 min. Cell suspensions were passed through a 114 Whatman filter paper (84). Spores were then resuspended at a density of 1.5×10^6 cells/ml in HL5 medium to induce germination and harvested for RNA isolation at various time points (10).

Polyphosphate gels. Polyphosphates gels (15% polyacrylamide [1610154; Bio-Rad], 7 M urea in Tris-borate-EDTA [TBE], 10% ammonium persulfate [APS], *N,N,N',N'*-tetramethylethylenediamine [TEMED]) were prerun for 30 min at 100 V with running buffer (89 mM Tris, 89 mM borate, 2 mM EDTA, pH 8.3). Wells were then rinsed with running buffer. Five micrograms of RNA for each sample was prepared with 6 \times loading dye (0.01% bromophenol blue, 30% glycerol, 10 mM Tris-HCl [pH 7.4], 1 mM

EDTA), loaded, and run on a polyphosphate gel at 150 V. PolyP 100 was used as a positive control. Gels were next rocked in staining solution (20% methanol, 2% glycerol, 20 mM Tris base, 2 μ g/ml DAPI) at room temperature for 30 min), followed by incubation in destain solution (20% methanol, 2% glycerol, 20 mM Tris base) for 45 min (10). For images, gels were exposed at 365 nm using an EpiChem³ Darkroom system (UVP Bioimaging Systems).

Western blotting. For Western blotting, protein samples were prepared by lysing 1×10^7 cells with NETN (0.5% Nonidet P-40, 150 mM NaCl, 50 mM Tris, and protease inhibitors [Roche Applied Science]), followed by sonication using an ultrasonic cell disruptor two times for 10 s on ice at 30% output. Protein concentration was determined by a bicinchoninic acid (BCA) assay, and then 10 μ g of protein was run on SDS-PAGE gels and transferred to a polyvinylidene difluoride (PVDF) membrane. Membranes were blocked with 5% milk in TBST (Tris-buffered saline, 0.1% Tween 20) and put in primary antibody at 1:1,000 overnight at 4°C. Secondary antibody was used at 1:5,000 at room temperature for 1 h.

Fluorescence recovery after photobleaching. FRAP analysis was performed as previously described (85). Briefly, a fluorescence recovery after photobleaching (FRAP) wizard on a Leica TCS Sp5 was used for photobleaching and recovery imaging. Imaging was performed at $\times 63$ magnification, and the region of interest was selected as half of a droplet. Bleaching was performed at 100% for 40 scans at 0.15 s. Baseline fluorescence and fluorescence recovery parameters were set as recommended by the FRAP wizard manual. Fluorescence intensity was analyzed using Fiji.

Sphericity. Z-stack images were used to render a 3D volume image using Imaris Software. Imaris surface creation wizard was then used to create a model of the 3D volume. A Gaussian filter and background subtraction were applied to improve the algorithm. Sphericity was then obtained using the statistics section in Imaris. Sphericity values were then plotted using GraphPad Prism.

Statistics. Statistics were performed using GraphPad Prism 8 software. Comparisons were made using a two-tailed *t* test for Fig. 4H and I. Error bars are standard deviations of the means. In all figure legends, *n* refers to the number of independent experiments performed.

ACKNOWLEDGMENTS

This work was supported by grants from the National Institutes of Health (R35 GM119544) and the National Ataxia Foundation to K.M.S. and F31 NS098754 to S.S. The funders had no role in the study design, data collection, data analysis, or in writing the manuscript.

K.M.S. and the Medical College of Wisconsin currently have a patent application submitted for commercial use of HSP48 bimolecular condensates.

S.S., A.F., and J.S. performed experiments. S.S. and K.M.S. designed the overall study. S.S. and K.M.S. wrote the manuscript. All authors analyzed the results and reviewed and edited the manuscript. All authors have read and approved the manuscript.

REFERENCES

- de Nadal E, Ammerer G, Posas F. 2011. Controlling gene expression in response to stress. *Nat Rev Genet* 12:833–845. <https://doi.org/10.1038/nrg3055>.
- Riback JA, Katanski CD, Kear-Scott JL, Pilipenko EV, Rojek AE, Sosnick TR, Drummond DA. 2017. Stress-triggered phase separation is an adaptive, evolutionarily tuned response. *Cell* 168:1028.e19–1040.e19. <https://doi.org/10.1016/j.cell.2017.02.027>.
- Wallace EW, Kear-Scott JL, Pilipenko EV, Schwartz MH, Laskowski PR, Rojek AE, Katanski CD, Riback JA, Dion MF, Franks AM, Airoidi EM, Pan T, Budnik BA, Drummond DA. 2015. Reversible, specific, active aggregates of endogenous proteins assemble upon heat stress. *Cell* 162:1286–1298. <https://doi.org/10.1016/j.cell.2015.08.041>.
- Wheeler JR, Matheny T, Jain S, Abrisch R, Parker R. 2016. Distinct stages in stress granule assembly and disassembly. *Elife* 5:e18413. <https://doi.org/10.7554/eLife.18413>.
- Nott TJ, Petsalaki E, Farber P, Jervis D, Fussner E, Plochowitz A, Craggs TD, Bazett-Jones DP, Pawson T, Forman-Kay JD, Baldwin AJ. 2015. Phase transition of a disordered nuage protein generates environmentally responsive membraneless organelles. *Mol Cell* 57:936–947. <https://doi.org/10.1016/j.molcel.2015.01.013>.
- Molliex A, Temirov J, Lee J, Coughlin M, Kanagaraj AP, Kim HJ, Mittag T, Taylor JP. 2015. Phase separation by low complexity domains promotes stress granule assembly and drives pathological fibrillization. *Cell* 163:123–133. <https://doi.org/10.1016/j.cell.2015.09.015>.
- Kroschwald S, Maharana S, Mateju D, Malinowska L, Nüske E, Poser I, Richter D, Alberti S. 2015. Promiscuous interactions and protein disaggregases determine the material state of stress-inducible RNP granules. *Elife* 4:e06807. <https://doi.org/10.7554/eLife.06807>.
- Suess PM, Watson J, Chen W, Gomer RH. 2017. Extracellular polyphosphate signals through Ras and Akt to prime *Dictyostelium discoideum* cells for development. *J Cell Sci* 130:2394–2404. <https://doi.org/10.1242/jcs.203372>.
- Suess PM, Gomer RH. 2016. Extracellular polyphosphate inhibits proliferation in an autocrine negative feedback loop in *Dictyostelium discoideum*. *J Biol Chem* 291:20260–20269. <https://doi.org/10.1074/jbc.M116.737825>.
- Livermore TM, Chubb JR, Saiardi A. 2016. Developmental accumulation of inorganic polyphosphate affects germination and energetic metabolism in *Dictyostelium discoideum*. *Proc Natl Acad Sci U S A* 113:996–1001. <https://doi.org/10.1073/pnas.1519440113>.
- Cotter DA, Raper KB. 1968. Properties of germinating spores of *Dictyostelium discoideum*. *J Bacteriol* 96:1680–1689.
- Boothby TC, Tapia H, Brozena AH, Piszkiwicz S, Smith AE, Giovannini I, Rebecchi L, Pielak GJ, Koshland D, Goldstein B. 2017. Tardigrades use intrinsically disordered proteins to survive desiccation. *Mol Cell* 65:975.e5–984.e5. <https://doi.org/10.1016/j.molcel.2017.02.018>.
- Schaap P. 2011. Evolutionary crossroads in developmental biology: *Dictyostelium discoideum*. *Development* 138:387–396. <https://doi.org/10.1242/dev.048934>.
- Fey P, Kowal AS, Gaudet P, Pilcher KE, Chisholm RL. 2007. Protocols for growth and development of *Dictyostelium discoideum*. *Nat Protoc* 2:1307–1316. <https://doi.org/10.1038/nprot.2007.178>.
- West CM, Erdos GW. 1990. Formation of the *Dictyostelium* spore coat. *Dev Genet* 11:492–506. <https://doi.org/10.1002/dvg.1020110526>.
- Santarriga S, Petersen A, Ndukwe K, Brandt A, Gerges N, Bruns Scaglione J, Scaglione KM. 2015. The social amoeba *Dictyostelium discoideum* is highly resistant to polyglutamine aggregation. *J Biol Chem* 290:25571–25578. <https://doi.org/10.1074/jbc.M115.676247>.

17. Malinowska L, Palm S, Gibson K, Verbavatz J-M, Alberti S. 2015. *Dictyostelium discoideum* has a highly Q/N-rich proteome and shows an unusual resilience to protein aggregation. *Proc Natl Acad Sci U S A* 112: E2620–E2629. <https://doi.org/10.1073/pnas.1504459112>.
18. Santarriaga S, Haver HN, Kanack AJ, Fikejs AS, Sison SL, Egner JM, Bostrom JR, Seminary ER, Hill RB, Link BA, Ebert AD, Scaglione KM. 2018. SRCP1 conveys resistance to polyglutamine aggregation. *Mol Cell* 71: 216.e7–228.e7. <https://doi.org/10.1016/j.molcel.2018.07.008>.
19. Morimoto RI. 1993. Cells in stress: transcriptional activation of heat shock genes. *Science* 259:1409–1410. <https://doi.org/10.1126/science.8451637>.
20. Sun Y, MacRae TH. 2005. Small heat shock proteins: molecular structure and chaperone function. *Cell Mol Life Sci* 62:2460–2476. <https://doi.org/10.1007/s00018-005-5190-4>.
21. Taylor RP, Benjamin IJ. 2005. Small heat shock proteins: a new classification scheme in mammals. *J Mol Cell Cardiol* 38:433–444. <https://doi.org/10.1016/j.yjmcc.2004.12.014>.
22. Riback JA, Katanski C, Kear-Scott JL, Sosnick TL, Drummond DA. 2017. Stress-triggered phase separation, tuned by unusual features of an intrinsically disordered region, promotes cellular fitness during stress. *FASEB J* 31 Suppl 1:914.2.
23. Franzmann TM, Jahnel M, Pozniakovskiy A, Mahamid J, Holehouse AS, Nüske E, Richter D, Baumeister W, Grill SW, Pappu RV, Hyman AA, Alberti S. 2018. Phase separation of a yeast prion protein promotes cellular fitness. *Science* 359:ea05654. <https://doi.org/10.1126/science.a05654>.
24. Chavali S, Gunnarsson A, Babu MM. 2017. Intrinsically disordered proteins adaptively reorganize cellular matter during stress. *Trends Biochem Sci* 42:410–412. <https://doi.org/10.1016/j.tibs.2017.04.007>.
25. Saad S, Cereghetti G, Feng Y, Picotti P, Peter M, Dechant R. 2017. Reversible protein aggregation is a protective mechanism to ensure cell cycle restart after stress. *Nat Cell Biol* 19:1202–1213. <https://doi.org/10.1038/ncb3600>.
26. Hyman AA, Weber CA, Juelicher F. 2014. Liquid-liquid phase separation in biology. *Annu Rev Cell Dev Biol* 30:39–58. <https://doi.org/10.1146/annurev-cellbio-100913-013325>.
27. Kato M, Han TW, Xie S, Shi K, Du X, Wu LC, Mirzaei H, Goldsmith EJ, Longgood J, Pei J, Grishin NV, Frantz DE, Schneider JW, Chen S, Li L, Sawaya MR, Eisenberg D, Tycko R, McKnight SL. 2012. Cell-free formation of RNA granules: low complexity sequence domains form dynamic fibers within hydrogels. *Cell* 149:753–767. <https://doi.org/10.1016/j.cell.2012.04.017>.
28. Patel A, Lee ZO, Jawerth L, Maharana S, Jahnel M, Hein MY, Stoyanov S, Mahamid J, Saha S, Franzmann TM, Pozniakovskiy A, Poser I, Maghelli N, Royer LA, Weigert M, Myers EW, Grill S, Drechsel D, Hyman AA, Alberti S. 2015. A liquid-to-solid phase transition of the ALS protein FUS accelerated by disease mutation. *Cell* 162:1066–1077. <https://doi.org/10.1016/j.cell.2015.07.047>.
29. Lin Y, Protter DS, Rosen MK, Parker R. 2015. Formation and maturation of phase-separated liquid droplets by RNA-binding proteins. *Mol Cell* 60:208–219. <https://doi.org/10.1016/j.molcel.2015.08.018>.
30. Liu G, Hu Y, Tunnacliffe A, Zheng Y. 2015. A plant cell model of polyglutamine aggregation: identification and characterisation of macromolecular and small-molecule anti-protein aggregation activity *in vivo*. *J Biotechnol* 207:39–46. <https://doi.org/10.1016/j.jbiotec.2015.05.003>.
31. Banani SF, Lee HO, Hyman AA, Rosen MK. 2017. Biomolecular condensates: organizers of cellular biochemistry. *Nat Rev Mol Cell Biol* 18: 285–298. <https://doi.org/10.1038/nrm.2017.7>.
32. Strom AR, Emelyanov AV, Mir M, Fyodorov DV, Darzacq X, Karpen GH. 2017. Phase separation drives heterochromatin domain formation. *Nature* 547:241–245. <https://doi.org/10.1038/nature22989>.
33. Bergeron-Sandoval L-P, Safaee N, Michnick SW. 2016. Mechanisms and consequences of macromolecular phase separation. *Cell* 165:1067–1079. <https://doi.org/10.1016/j.cell.2016.05.026>.
34. Aguzzi A, Altmeyer M. 2016. Phase separation: linking cellular compartmentalization to disease. *Trends Cell Biol* 26:547–558. <https://doi.org/10.1016/j.tcb.2016.03.004>.
35. Xiang S, Kato M, Wu LC, Lin Y, Ding M, Zhang Y, Yu Y, McKnight SL. 2015. The LC domain of hnRNP A2 adopts similar conformations in hydrogel polymers, liquid-like droplets, and nuclei. *Cell* 163:829–839. <https://doi.org/10.1016/j.cell.2015.10.040>.
36. Murakami T, Qamar S, Lin JQ, Schierle GSK, Rees E, Miyashita A, Costa AR, Dodd RB, Chan FTS, Michel CH, Kronenberg-Versteeg D, Li Y, Yang S-P, Wakutani Y, Meadows W, Ferry RR, Dong L, Tartaglia GG, Favrin G, Lin W-L, Dickson DW, Zhen M, Ron D, Schmitt-Ulms G, Fraser PE, Shneider NA, Holt C, Vendruscolo M, Kaminski CF, St George-Hyslop P. 2015. ALS/FTD mutation-induced phase transition of FUS liquid droplets and reversible hydrogels into irreversible hydrogels impairs RNP granule function. *Neuron* 88:678–690. <https://doi.org/10.1016/j.neuron.2015.10.030>.
37. Pak CW, Kosno M, Holehouse AS, Padrick SB, Mittal A, Ali R, Yunus AA, Liu DR, Pappu RV, Rosen MK. 2016. Sequence determinants of intracellular phase separation by complex coacervation of a disordered protein. *Mol Cell* 63:72–85. <https://doi.org/10.1016/j.molcel.2016.05.042>.
38. Altmeyer M, Neelens KJ, Teloni F, Pozdnyakova I, Pellegrino S, Gröfte M, Rask M-BD, Streicher W, Jungmichel S, Nielsen ML, Lukas J. 2015. Liquid demixing of intrinsically disordered proteins is seeded by poly(ADP-ribose). *Nat Commun* 6:8088. <https://doi.org/10.1038/ncomms9088>.
39. Ambadipudi S, Biernat J, Riedel D, Mandelkow E, Zweckstetter M. 2017. Liquid-liquid phase separation of the microtubule-binding repeats of the Alzheimer-related protein Tau. *Nat Commun* 8:275. <https://doi.org/10.1038/s41467-017-00480-0>.
40. Wegmann S, Eftekharzadeh B, Tepper K, Zoltowska KM, Bennett RE, Dujardin S, Laskowski PR, MacKenzie D, Kamath T, Commins C, Vanderburg C, Roe AD, Fan Z, Molliex AM, Hernandez-Vega A, Muller D, Hyman AA, Mandelkow E, Taylor JP, Hyman BT. 2018. Tau protein liquid-liquid phase separation can initiate tau aggregation. *EMBO J* 37:e98049. <https://doi.org/10.15252/emboj.201798049>.
41. Boeynaems S, Bogaert E, Kovacs D, Konijnenberg A, Timmerman E, Volkov A, Guharoy M, De Decker M, Jaspers T, Ryan VH, Janke AM, Baatsen P, Vercruyse T, Kolaitis R-M, Daelemans D, Taylor JP, Kedersha N, Anderson P, Impens F, Sobott F, Schymkowitz J, Rousseau F, Fawzi NL, Robberecht W, Van Damme P, Tompa P, Van Den Bosch L. 2017. Phase separation of C9orf72 dipeptide repeats perturbs stress granule dynamics. *Mol Cell* 65:1044.e5–1055.e5. <https://doi.org/10.1016/j.molcel.2017.02.013>.
42. Zhang H, Gómez-García MR, Brown MRW, Kornberg A. 2005. Inorganic polyphosphate in *Dictyostelium discoideum*: influence on development, sporulation, and predation. *Proc Natl Acad Sci U S A* 102:2731–2735. <https://doi.org/10.1073/pnas.0500023102>.
43. Cremers CM, Knoefler D, Gates S, Martin N, Dahl J-U, Lempart J, Xie L, Chapman MR, Galvan V, Southworth DR, Jakob U. 2016. Polyphosphate: a conserved modifier of amyloidogenic processes. *Mol Cell* 63:768–780. <https://doi.org/10.1016/j.molcel.2016.07.016>.
44. Gray MJ, Wholey WY, Wagner NO, Cremers CM, Mueller-Schickert A, Hock NT, Krieger AG, Smith EM, Bender RA, Bardwell JC, Jakob U. 2014. Polyphosphate is a primordial chaperone. *Mol Cell* 53:689–699. <https://doi.org/10.1016/j.molcel.2014.01.012>.
45. Henriques AO, Beall BW, Moran CP, Jr. 1997. CotM of *Bacillus subtilis*, a member of the alpha-crystallin family of stress proteins, is induced during development and participates in spore outer coat formation. *J Bacteriol* 179:1887–1897. <https://doi.org/10.1128/jb.179.6.1887-1897.1997>.
46. Reischl S, Thake S, Homuth G, Schumann W. 2001. Transcriptional analysis of three *Bacillus subtilis* genes coding for proteins with the alpha-crystallin domain characteristic of small heat shock proteins. *FEMS Microbiol Lett* 194:99–103. <https://doi.org/10.1111/j.1574-6968.2001.tb09453.x>.
47. Sontag EM, Samant RS, Frydman J. 2017. Mechanisms and functions of spatial protein quality control. *Annu Rev Biochem* 86:97–122. <https://doi.org/10.1146/annurev-biochem-060815-014616>.
48. Elbaum-Garfinkle S. 2019. Matter over mind: liquid phase separation and neurodegeneration. *J Biol Chem* 294:7160–7168. <https://doi.org/10.1074/jbc.REV118.001188>.
49. Alberti S, Gladfelter A, Mittag T. 2019. Considerations and challenges in studying liquid-liquid phase separation and biomolecular condensates. *Cell* 176:419–434. <https://doi.org/10.1016/j.cell.2018.12.035>.
50. Jain S, Wheeler R, Walters RW, Agrawal A, Barsic A, Parker R. 2016. ATPase-modulated stress granules contain a diverse proteome and substructure. *Cell* 164:487–498. <https://doi.org/10.1016/j.cell.2015.12.038>.
51. Das RK, Pappu RV. 2013. Conformations of intrinsically disordered proteins are influenced by linear sequence distributions of oppositely charged residues. *Proc Natl Acad Sci U S A* 110:13392–13397. <https://doi.org/10.1073/pnas.1304749110>.
52. Zhang H, Elbaum-Garfinkle S, Langdon EM, Taylor N, Occhipinti P, Bridges AA, Brangwynne CP, Gladfelter AS. 2015. RNA controls polyQ protein phase transitions. *Mol Cell* 60:220–230. <https://doi.org/10.1016/j.molcel.2015.09.017>.

53. King OD, Gitler AD, Shorter J. 2012. The tip of the iceberg: RNA-binding proteins with prion-like domains in neurodegenerative disease. *Brain Res* 1462:61–80. <https://doi.org/10.1016/j.brainres.2012.01.016>.
54. Kwon I, Kato M, Xiang S, Wu L, Theodoropoulos P, Mirzaei H, Han T, Xie S, Corden JL, McKnight SL. 2013. Phosphorylation-regulated binding of RNA polymerase II to fibrous polymers of low-complexity domains. *Cell* 155:1049–1060. <https://doi.org/10.1016/j.cell.2013.10.033>.
55. Nielsen FC, Hansen HT, Christiansen J. 2016. RNA assemblages orchestrate complex cellular processes. *Bioessays* 38:674–681. <https://doi.org/10.1002/bies.201500175>.
56. Tuvshinjargal N, Lee W, Park B, Han K. 2016. PRIdictor: Protein-RNA Interaction predictor. *Biosystems* 139:17–22. <https://doi.org/10.1016/j.biosystems.2015.10.004>.
57. Kanehisa M, Goto S, Kawashima S, Nakaya A. 2002. The KEGG databases at GenomeNet. *Nucleic Acids Res* 30:42–46. <https://doi.org/10.1093/nar/30.1.42>.
58. Jimenez-Nunez MD, Moreno-Sanchez D, Hernandez-Ruiz L, Benitez-Rondan A, Ramos-Amaya A, Rodriguez-Bayona B, Medina F, Brieua JA, Ruiz FA. 2012. Myeloma cells contain high levels of inorganic polyphosphate which is associated with nucleolar transcription. *Haematologica* 97:1264–1271. <https://doi.org/10.3324/haematol.2011.051409>.
59. McInerney P, Mizutani T, Shiba T. 2006. Inorganic polyphosphate interacts with ribosomes and promotes translation fidelity *in vitro* and *in vivo*. *Mol Microbiol* 60:438–447. <https://doi.org/10.1111/j.1365-2958.2006.05103.x>.
60. Rao NN, Gómez-García MR, Kornberg A. 2009. Inorganic polyphosphate: essential for growth and survival. *Annu Rev Biochem* 78:605–647. <https://doi.org/10.1146/annurev.biochem.77.083007.093039>.
61. Otto GP, Wu MY, Kazgan N, Anderson OR, Kessin RH. 2004. *Dictyostelium* macroautophagy mutants vary in the severity of their developmental defects. *J Biol Chem* 279:15621–15629. <https://doi.org/10.1074/jbc.M311139200>.
62. Otto GP, Wu MY, Kazgan N, Anderson OR, Kessin RH. 2003. Macroautophagy is required for multicellular development of the social amoeba *Dictyostelium discoideum*. *J Biol Chem* 278:17636–17645. <https://doi.org/10.1074/jbc.M212467200>.
63. Lindsey DF, Amerik A, Deery WJ, Bishop JD, Hochstrasser M, Gomer RH. 1998. A deubiquitinating enzyme that disassembles free polyubiquitin chains is required for development but not growth in *Dictyostelium*. *J Biol Chem* 273:29178–29187. <https://doi.org/10.1074/jbc.273.44.29178>.
64. Sawarkar R, Roy N, Rao S, Raman S, Venkatesh S, Suguna K, Tatu U. 2008. Heat shock protein 90 regulates development in *Dictyostelium discoideum*. *J Mol Biol* 383:24–35. <https://doi.org/10.1016/j.jmb.2008.08.006>.
65. Moerman AM, Klein C. 1997. Developmental regulation of Hsp32, a small heat shock protein in *Dictyostelium discoideum*. *Exp Cell Res* 237:149–157. <https://doi.org/10.1006/excr.1997.3774>.
66. Grousl T, Ungelenk S, Miller S, Ho C-T, Khokhrina M, Mayer MP, Bukau B, Mogk A. 2018. A prion-like domain in Hsp42 drives chaperone-facilitated aggregation of misfolded proteins. *J Cell Biol* 217:1269–1285. <https://doi.org/10.1083/jcb.201708116>.
67. Hnisz D, Shrinivas K, Young RA, Chakraborty AK, Sharp PA. 2017. A phase separation model for transcriptional control. *Cell* 169:13–23. <https://doi.org/10.1016/j.cell.2017.02.007>.
68. Simpson-Lavy K, Xu T, Johnston M, Kupiec M. 2017. The Std1 activator of the Snf1/AMPK kinase controls glucose response in yeast by a regulated protein aggregation. *Mol Cell* 68:1120.e3–1133.e3. <https://doi.org/10.1016/j.molcel.2017.11.016>.
69. Conicella AE, Zerze GH, Mittal J, Fawzi NL. 2016. ALS mutations disrupt phase separation mediated by alpha-helical structure in the TDP-43 low-complexity C-terminal domain. *Structure* 24:1537–1549. <https://doi.org/10.1016/j.str.2016.07.007>.
70. McGurk L, Gomes E, Guo L, Mojsilovic-Petrovic J, Tran V, Kalb RG, Shorter J, Bonini NM. 2018. Poly(ADP-ribose) prevents pathological phase separation of TDP-43 by promoting liquid demixing and stress granule localization. *Mol Cell* 71:703.e9–717.e9. <https://doi.org/10.1016/j.molcel.2018.07.002>.
71. Li H-R, Chiang W-C, Chou P-C, Wang W-J, Huang J-R. 2018. TAR DNA-binding protein 43 (TDP-43) liquid-liquid phase separation is mediated by just a few aromatic residues. *J Biol Chem* 293:6090–6098. <https://doi.org/10.1074/jbc.AC117.001037>.
72. Mackenzie IR, Nicholson AM, Sarkar M, Messing J, Purice MD, Pottier C, Annu K, Baker M, Perkerson RB, Kurti A, Matchett BJ, Mittag T, Temirov J, Hsiung G-YR, Krieger C, Murray ME, Kato M, Fryer JD, Petrucelli L, Zinman L, Weintraub S, Mesulam M, Keith J, Zivkovic SA, Hirsch-Reinshagen V, Roos RP, Züchner S, Graff-Radford NR, Petersen RC, Caselli RJ, Wszolek ZK, Finger E, Lippa C, Lacomis D, Stewart H, Dickson DW, Kim HJ, Rogaeve E, Bigio E, Boylan KB, Taylor JP, Rademakers R. 2017. TIA1 mutations in amyotrophic lateral sclerosis and frontotemporal dementia promote phase separation and alter stress granule dynamics. *Neuron* 95:808.e9–816.e9. <https://doi.org/10.1016/j.neuron.2017.07.025>.
73. Blair LJ, Nordhues BA, Hill SE, Scaglione KM, O'Leary JC, Fontaine SN, Breydo L, Zhang B, Li P, Wang L, Cotman C, Paulson HL, Muschol M, Uversky VN, Klengel T, Binder EB, Kaye R, Golde TE, Berchtold N, Dickey CA. 2013. Accelerated neurodegeneration through chaperone-mediated oligomerization of tau. *J Clin Invest* 123:4158–4169. <https://doi.org/10.1172/JCI69003>.
74. Peskett TR, Rau F, O'Driscoll J, Patani R, Lowe AR, Saibil HR. 2018. A liquid to solid phase transition underlying pathological huntingtin exon1 aggregation. *Mol Cell* 70:588.e6–601.e6. <https://doi.org/10.1016/j.molcel.2018.04.007>.
75. Munder MC, Midtvedt D, Franzmann T, Nüske E, Otto O, Herbig M, Ulbricht E, Müller P, Taubenberger A, Maharana S, Malinowska L, Richter D, Guck J, Zaburdaev V, Alberti S. 2016. A pH-driven transition of the cytoplasm from a fluid- to a solid-like state promotes entry into dormancy. *Elife* 5:e09347. <https://doi.org/10.7554/eLife.09347>.
76. Joyner RP, Tang JH, Helenius J, Dultz E, Brune C, Holt LJ, Huet S, Muller DJ, Weis K. 2016. A glucose-starvation response regulates the diffusion of macromolecules. *Elife* 5:e09376. <https://doi.org/10.7554/eLife.09376>.
77. Parry BR, Surovtsev IV, Cabeen MT, O'Hern CS, Dufresne ER, Jacobs-Wagner C. 2014. The bacterial cytoplasm has glass-like properties and is fluidized by metabolic activity. *Cell* 156:183–194. <https://doi.org/10.1016/j.cell.2013.11.028>.
78. Höfheld J. 2017. Preserving protein function through reversible aggregation. *Nat Cell Biol* 19:1142–1144. <https://doi.org/10.1038/ncb3620>.
79. Docampo R, de Souza W, Miranda K, Rohloff P, Moreno SN. 2005. Acidocalcins - conserved from bacteria to man. *Nat Rev Microbiol* 3:251–261. <https://doi.org/10.1038/nrmicro1097>.
80. Tocheva EI, Dekas AE, McGlynn SE, Morris D, Orphan VJ, Jensen GJ. 2013. Polyphosphate storage during sporulation in the Gram-negative bacterium *Acetonebma longum*. *J Bacteriol* 195:3940–3946. <https://doi.org/10.1128/JB.00712-13>.
81. Knecht D, Pang KM. 1995. Electroporation of *Dictyostelium discoideum*. *Methods Mol Biol* 47:321–330.
82. Pang KM, Lynes MA, Knecht DA. 1999. Variables controlling the expression level of exogenous genes in *Dictyostelium*. *Plasmid* 41:187–197. <https://doi.org/10.1006/plas.1999.1391>.
83. Levi S, Polyakov M, Egelhoff TT. 2000. Green fluorescent protein and epitope tag fusion vectors for *Dictyostelium discoideum*. *Plasmid* 44:231–238. <https://doi.org/10.1006/plas.2000.1487>.
84. Chiew YY, Reimers JM, Wright BE. 1985. Steady state models of spore cell metabolism in *Dictyostelium discoideum*. *J Biol Chem* 260:15325–15331.
85. Petersen A, Gerges NZ. 2015. Neurogranin regulates CaM dynamics at dendritic spines. *Sci Rep* 5:11135. <https://doi.org/10.1038/srep11135>.